Hand-Eye Calibration

S. Rémy, M. Dhome, J.M Lavest, N. Daucher

Laboratoire des Sciences et Matériaux pour l'Electronique, et d'Automatique (LASMEA)
URA 1793 du CNRS, Université Blaise-Pascal de Clermont-Ferrand
e-mail : remy@le-eva.univ-bpclermont.fr

Abstract

This paper deals with the hand-eye calibration problem. The question is to find the relative position and orientation between a camera rigidly mounted on the robot last joint and the gripper. Hand-eye calibration is useful in many cases as for example, grasping objects or reconstructing 3D scenes. Almost all existing solutions lead to solve for homogeneous transformation equations of the form $AX = XB$. We propose a new formulation. Our method determines simultaneously the hand-eye transformation and the location of a calibration object with respect to the robot world coordinate system. The main advantage is that the number of unknows remains constant and the solution is constrainted to be consistent with the whole set of calibration data.

Results of simulation experiments and comparisons with classical techniques are reported and analysed. Real experiments with a Cartesian robot are described and the results accuracy discussed.

1 Introduction

In order to control the displacements of a robot by a camera mounted on its hand, it is important to determine the relative positions and orientations of the camera and hand frames. This problem is known as the *hand-eye calibration problem.* As well described in [2], [3], [1], hand-eye calibration is useful in two kinds of tasks at least:

- *Generate proper movements into the workspace frame in order to grasp an object.* In this case, an accurate step of recognition and location is required to determine the position and orientation of the object in the camera coordinate system. Then, if the hand-eye transformation is rightly identified, the object location can easily be given into the robot base coordinate system, allowing the robot to move and grasp it.
- *Accurate displacement of the sensor* : can be required for some particular tasks as reconstructing 3D scenes or using vision to provide 3D informations about an object. In these special cases, the relative positions of the sensor in the workspace need to be known and therefore hand-eye calibration must be previously performed.

Almost all existing solutions of the hand-eye calibration problem lead to solve an homogeneous transformation equation of the form:

$$AX = XB \tag{1}$$

where X is unknown and represents the relative position and orientation between the sensor frame and the robot hand. In the particular case in which the sensor is a camera, the X transformation is defined between the camera and the robot hand coordinate system.

The basic set-up for the hand-eye calibration can be described as follows.

The robot with the camera fixed on its hand makes a series of n displacements inside its workspace. At the pause between each motion, the camera acquires an image of a calibration object. Therefore solving $A_iX = XB_i, i \in [1..n]$ requires to estimate the rotational and translational components of the n locations of the calibration object and those of the hand-eye transform.

Transformation B is obtained using two robot hand positions (provided by robot optical encoders) and transformation A is determined using two object locations in the camera coordinate system. Both transformation A and B include measurement errors due to mechanical defects and noise affecting the data.

Using a set of n robot positions, there is several classical ways as closed form solutions (solving rotational then translational parameters of the transform)

Proc. IROS 97 0-7803-4119-8/97/$10©1997 IEEE

or non linear optimization approach (solving simultaneously rotational and translational parts) to find the best hand-eye transformation X that minimizes $(A_iX = XB_i)$. But, at the solution, the calibration object location in the robot workspace may be inconsistent with the image content.

This article has the following main contributions:

- First of all, we propose a new formulation of the hand-eye calibration problem, where the total number of unknown parameters remains constant and equal to 12, whatever the total number of robot positions is. These 12 parameters are those of two homogeneous transformations : the first six parameters represents the hand-eye transformation, the other six are the location of the calibration object in the robot coordinate system.

- Secondly, this new formulation allows to express the 12 unknown parameters in a sum of scalar products, which correspond to a distance between a 3D point of the calibration object and a plane defined from image data.

The article is organized as follows:

In a first part, the new formulation of the hand-eye calibration process is described. In a second part, results of simulation are reported. Their analysis allows to test the reliability of the new formulation compared with well known algorithms described in the literature. Finally the results of a real hand-eye calibration experiment on a Cartesian robot are given.

2 Hand-Eye Calibration: a New Formulation

2.1 Coordinate Systems Definitions

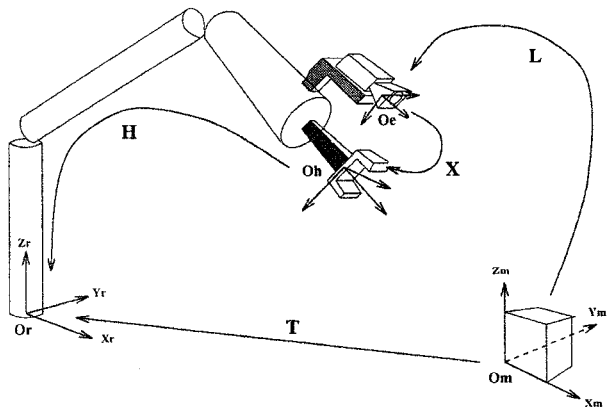

Figure 1: Coordinate systems definitions

To solve for the hand-eye calibration problem requires to define a set of coordinate frames. Here is a list of the different systems we use :

- $F_r : (O_r, X_r, Y_r, Z_r)$ is the robot world coordinate frame. It is situated inside the robot workspace. All other frames are located with respect to it and in particular, the location of the hand frame relative to the robot world system is constantly provided by the robot encoders outputs.

- $F_m : (O_m, X_m, Y_m, Z_m)$ is the calibration object coordinate system. All calibration object points are referenced with respect to this frame.

- $F_h : (O_h, X_h, Y_h, Z_h)$ is the hand coordinate system. It may be either the gripper's frame (if there is a fixed gripper) or the coordinate system related to the robot link where the gripper is usually fastened.

- $F_e : (O_e, X_e, Y_e, Z_e)$ is the camera coordinate frame. Its origin is located at the optical center of the vision system. Its Z_e axis coincides with the optical axis of the camera and the X_e and Y_e axes are parallel to the image lines and rows. A classical calibration of the intrinsic camera parameters allows to express the image informations relative to the F_e frame.

These coordinate systems are related to each other by a set of homogeneous transformation matrices, which are listed below.

- Let H be the homogeneous matrix which defines coordinate transformation from F_h to F_r i.e H gives the position and orientation of F_h with respect to F_r. H is a (4×4) matrix which is composed by a rotational part (a (3×3) rotational matrix), denoted R_h and a translational part (a (3×1) translation vector), denoted T_h.

  H will be written as follows :

$$H = \begin{pmatrix} R_h & T_h \\ 0 & 1 \end{pmatrix} \quad (2)$$

  Note that H components for each position and orientation of the gripper are directly supplied by the outputs of the robot encoders.

- L : homogeneous transformation matrix from F_m to F_e.

  L must be computed by performing extrinsic calibration. However, it should be stressed that the extrinsic calibration is in most cases greatly dependent on intrinsic parameters calibration and

image detections. So, L estimation might be sometimes quite inaccurate.

$$L = \begin{pmatrix} R_l & T_l \\ 0 & 1 \end{pmatrix} \quad (3)$$

- T : homogeneous transformation matrix from F_m to F_r.

  T represents the location of the calibration object in the robot world coordinate sytem.

$$T = \begin{pmatrix} R_t & T_t \\ 0 & 1 \end{pmatrix} \quad (4)$$

- X : homogeneous transformation matrix from F_e to F_h is the unknown hand-eye transformation.

$$X = \begin{pmatrix} R_x & T_x \\ 0 & 1 \end{pmatrix} \quad (5)$$

Figure 1 explains the relationships between the different frames and the various homogeneous matrices.

2.2 Classical Approach

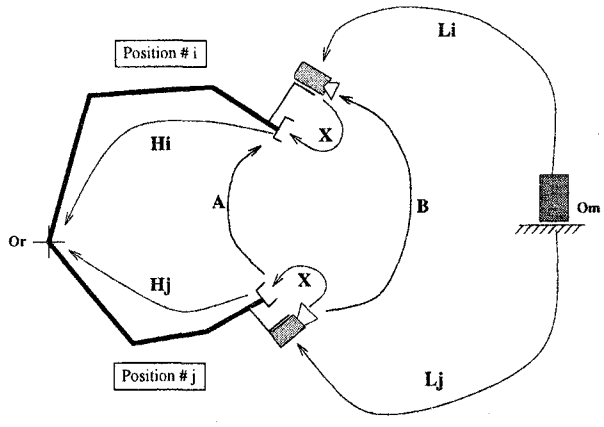

Figure 2: Classical approach

Let's consider two different positions i and j of the gripper inside the robot workspace (see fig.2).

Then, matrices H and L have to be indexed by i and j corresponding to these two different stations of the gripper. Matrix X doesn't have any index since the camera is rigidly mounted on one of the robot links.

As H_i and H_j are known, it is possible to estimate the transformation A that gives the location of the second gripper position relative to the first position.

$$A = (H_i)^{-1}(H_j) \quad (6)$$

Similarly, L_i and L_j can be computed and it is also possible to determine B :

$$B = (L_i)(L_j)^{-1} \quad (7)$$

According to the figure 2, it is obvious that

$$AX = XB \quad (8)$$

where A and B are known and X represents the hand-eye calibration transformation that is to be estimated.

At least three different robot motions are necessary to solve the system [3]. In practice, a set of n positions ($n \geq 3$) is selected and the system is overdetermined.

There is a lot of possibilities to solve for

$$(A_i X = X B_i) \quad i \in [1..n] \quad (9)$$

[2] and [3] propose closed-form solutions. These methods determine independently the rotational and the translational parts of X. More recently [1] proposed a non linear optimization technique to solve simultaneously for R_x and T_x. This latter formulation seems to be significantly less sensitive to noise than the previous solutions.

In all cases, these methods require to compute the rotational and translational components of the location matrices L_i at each position of the gripper, which represents at least $6 \times n$ unknowns, plus 6 others parameters for X.

2.3 A New Approach

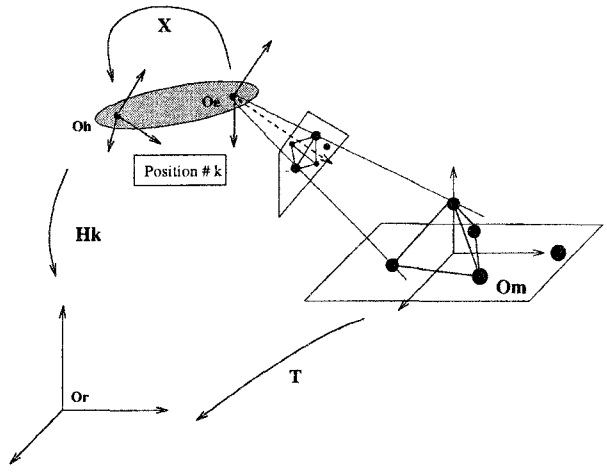

Figure 3: New formulation

In this section, we propose a new formulation for the hand-eye calibration problem. The basic set-up remains the same than in the classical approaches and we consider a series of n gripper motions with the camera acquiring an image at each pause.

Under these conditions, it is possible to write a set of N equations that depend on the unknown homogeneous transformations X and T, defined in section 2.1.

The problem is now : given a set of n robot positions (see fig.3), find the best transformations X and T so that the calibration object location in the robot workspace (T) could be consistent with its perspective projection in the n viewpoints.

The advantage of this formulation is that for each position k, the corresponding equation takes directly the image data into account. Thus, it guarantees X and T to be the more consistent estimations with the sets of calibration points and gripper positions.

Moreover, if the rotational part of the transformation is expressed as three Euler's angles, the total number of parameters to be estimated remains constant and equal to 12, whatever the total number of robot hand positions is. These 12 parameters are composed of the three Euler's angles and the three components of the translation vector of X and T respectively. They are denoted : $(\alpha_x, \beta_x, \gamma_x, u_x, v_x, w_x)$ and $(\alpha_t, \beta_t, \gamma_t, u_t, v_t, w_t)$.

The Error Function. The calibration object is a regular tetrahedron for which each vertex is marked by a LED. It comprises an extra LED lying on the base plane which creates an assymetry and which is used to recognize the viewpoint. The geometrical model of this object needs to be very precisely measured. It will be described more completely in the next section.

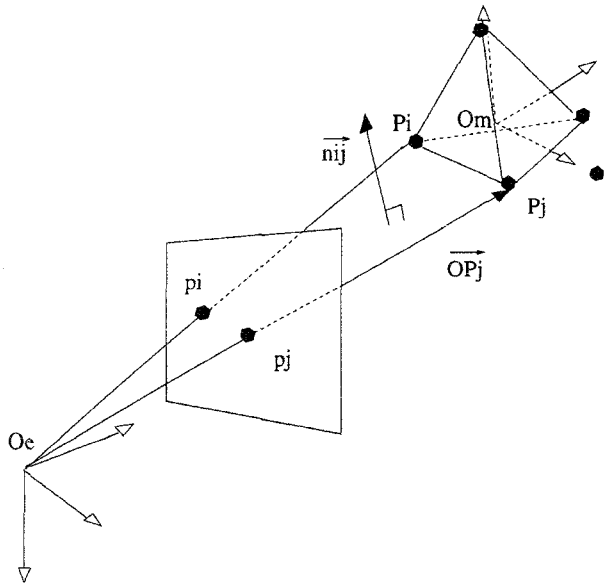

Figure 4: *interpretation plane*

For each image and for each 3D point of the calibration target, we can define an *interpretation plane* (see fig.4).

Let's P_i and P_j be two 3D points of the calibration object and p_i and p_j their projective projections. p_i and p_j belong to the image plane. The *interpretation plane* of P_i, denoted Π_i, is defined by p_i, p_j and O_e, the camera lens center. Note that, by definition, Π_i is as well the *interpretation plane* of P_j so it will be denoted Π_{ij}.

For one image and a calibration object with five points, there is 10 different *interpretation planes*. They can be represented by their normal vector $\overrightarrow{n_{ij}^e}$ which is the cross product:

$$\overrightarrow{n_{ij}^e} = \frac{\overrightarrow{O_e^e p_i^e} \wedge \overrightarrow{O_e^e p_j^e}}{||\overrightarrow{O_e^e p_i^e} \wedge \overrightarrow{O_e^e p_j^e}||} \tag{10}$$

In all the following equations, the upper lowercase letters '$*$' recall that the coordinates of the so indexed point or vector are expressed in the '$*$' coordinate frame (F_*).

The distance between P_j and its *interpretation plane*, Π_{ij}, is given by the scalar product Q_{ij}^e :

$$Q_{ij}^e = \overrightarrow{n_{ij}^e} \cdot \overrightarrow{O_e^e P_j^e}. \tag{11}$$

It is clear that distance Q_{ij}^e must be equal to zero since P_j^e belongs to Π_{ij}.

Expressing Q_{ij}^e in the robot world coordinate frame will lead the unknown transformations X and T to appear in (11).

We have :

$$Q_{ij}^r = \overrightarrow{n_{ij}^r} \cdot \overrightarrow{O_e^r P_j^r} \tag{12}$$

$$\textit{where} \quad \left.\begin{array}{l} \overrightarrow{n_{ij}^r} = (H \cdot X) \cdot \overrightarrow{n_{ij}^e} \\ O_e^r = (H \cdot X) \cdot O_e^e \\ P_j^r = T \cdot P_j^m \end{array}\right\} \tag{13}$$

$$\Longrightarrow \overrightarrow{O_e^r P_j^r} = T \cdot P_j^m - (H \cdot X) \cdot O_e^e$$

Rewriting (13) with the notations introduced in section 2.1 causes the rotational and translational parts of the homogeneous transformations to appear explicitly in the equations. Then we have :

$$\left.\begin{array}{l} \overrightarrow{n_{ij}^r} = (R_h \cdot R_x) \cdot \overrightarrow{n_{ij}^e} \\ O_e^r = R_h \cdot T_x + T_h \\ P_j^r = R_t \cdot P_j^m + T_t \end{array}\right\} \tag{14}$$

$$\Longrightarrow \overrightarrow{O_e^r P_j^r} = R_t \cdot P_j^m + T_t - R_h \cdot T_x - T_h \tag{15}$$

Substituting this into (12) we have :

$$Q_{ij}^r = [(R_h R_x) \cdot \overrightarrow{n_{ij}^e}] \cdot [R_t \cdot P_j^m + T_t - R_h \cdot T_x - T_h] \tag{16}$$

where $\overrightarrow{n_{ij}^e}$ are computed from the image points, P_j^m are the tetrahedron 3D points and R_h and T_h are given by the robot encoders outputs for each position k.

For one station of the gripper, we can write 20 equations of the form (16). Thus, we obtain a total of $(20 \times n = N)$ equations for a series of n stations.

Solving for the transformations X and T is then equivalent to minimize the positive error function :

$$e(X,T) = \sum_{k=1}^{N} (Q_{ij}^r)_k^2 \qquad (17)$$

with respect to

- $(\alpha_x, \beta_x, \gamma_x)$ Euler's angles of R_x,
- (u_x, v_x, w_x) components of T_x,
- $(\alpha_t, \beta_t, \gamma_t)$ Euler's angles of R_t,
- (u_t, v_t, w_t) components of T_t.

This error function is non linear and the minimization will be performed using a Levenberg-Marquardt method.

3 Results of the Simulation Experiments

To improve the reliability of our method for the hand-eye calibration problem, we have performed three sequences of simulation experiments.

Simulations present two major advantages. On one hand, it allows us to control the uncertainties occuring in the calibration set-up which include the generation of series of robot motions and synthetical corresponding images, and then to see their effect on the final results accuracy. On the other hand, it enables to compare our results with those given by other algorithms working on the same data sets.

Comparison between various hand-eye calibration processes was already performed and reported in two papers at least [4] and [1].

Wang [4] has tested in particular the Shiu/Ahmad method [2] in comparison with the Tsai/Lenz method [3]. He concludes that both procedures achieve consistent results, but that the Tsai/Lenz process produces on average the smallest standard deviations.

In [1], Horaud and Dornaika present a closed-form solution and a non linear optimization technique for performing hand-eye calibration. They compare these new processes with the Tsai/Lenz method which was up to now the more stable one. They conclude that the non linear optimization resists better to noise than the both other ones. So, we have chosen to test our results in comparison with the non linear optimization solutions.

To generate simulation data, we have first simulated a series of n motions of the gripper in the robot workspace. These movements are as realistic as possible since they are calculated with the Jacobian matrix of the Cartesian robot of the laboratory.

Transformations X and T have been fixed and the numerical values of their Euler's angles and translation components are the following :

$\alpha_x = 20^o$, $u_x = 0.136m$; $\alpha_t = 0^o$, $u_t = 2.0m$;
$\beta_x = 15^o$, $v_x = 0.076m$; $\beta_t = 0^o$, $v_t = 2.0m$;
$\gamma_x = 160^o$, $w_x = 0.188m$; $\gamma_t = 0^o$, $w_t = 2.0m$.

The global robot movement includes translations along the X_e, Y_e and Z_e axes of the camera coordinate frame F_e and a set of displacements on a sphere which is centered in O_m and has a 1 meter radius. The entire series of motions is chosen so that the fixed calibration target remains in the camera's view.

Each series is composed of 18 simulated moves and 18 synthetical images.

Each move, generated without any error, is in a second time perturbed by adding noises on the position and orientation of the gripper i.e the Euler's angles and the translation components of H. These noises are random numbers distributed according to normal Gaussian distributions. The means of these distributions are the parameters values $(\alpha_h, \beta_h, \gamma_h, u_h, v_h, w_h)$ and the standard deviations are fixed for each different simulations. They are listed in table 1.

The calibration object is the regular tetrahedron mentioned in section 2.3.1. Its base belongs to a rectangular plate of $14.0cm \times 6.6cm$ including 4 LEDs. 3 of these LEDs are forming an equilateral triangle of $5.0cm$ side. This triangle is the base of the tetrahedron. The plate is surmounted by an axis of $4.0cm$ height. The fifth LED is fixed at the top of this axis and is the last vertex of the tetrahedron. The set of synthetical images are produced with the geometrical model of this object.

The image data corresponding to each gripper station are also perturbed. For this purpose, we have taken into account the uncertainties provided by intrinsic calibration and noises due to the image feature coordinates extractions. We have also considered that these defects were distributed according to normal Gaussian laws. The standard deviations of these distributions are listed in table 2.

The global simulation experiment comprises 3 sequences of 100 series with different values of noise. The magnitude of the noise standard deviations increases from sequence #1 to sequence #3 for the H parameters. The uncertainties on the camera intrinsic parameters i.e the optical center, the focal length and the scale factor, and on the image points remain the same for all simulations (see table 2).

For each series, we have calculated the deviation between the theoritical values of X parameters (listed above) and the solutions provided by our algorithm

sequence #	1	2	3
σ_{noise} (degree) Euler's angles of H	0.1	0.5	1.0
σ_{noise} (mm) translation components of H	0.1	1.0	10.0

Table 1: Standard deviations of noise for H parameters

	image points (pixel)	image center (pixel)	focal length (pixel)	scale factor (%)
σ_{noise}	2.0	5.0	10.0	1.0

Table 2: Standard deviations of noise for image points and intrinsic parameters

(simultaneous estimation of X and T) and the deviation between the theoritical values of X parameters and the solutions of the non linear optimization process [1]. We made then a statistical study and the results reported for each sequence are the averages and the standard deviations of these differences.

Figures 5 and 6 illustrate the comparison for all the estimated parameters and the 3 sequences. Results of the simultaneous estimation of X and T are marked by $\diamond$ and those of the non linear optimization technique by $\square$.

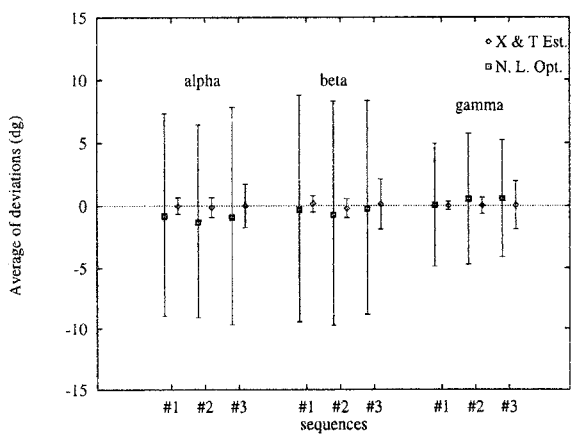

Figure 5: Evolution of α_x, β_x and γ_x errors with the both methods.

Whatever the considered parameter and the considered sequence are, the errors are always more significant for the non linear optimization results. For example, α_x errors are always smaller than 1 degree for the simultaneous estimation of X and T and about

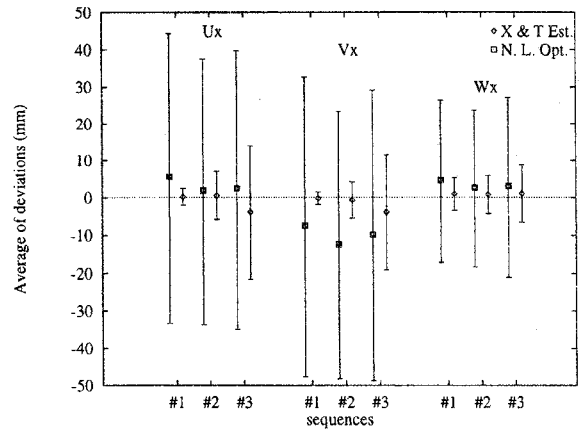

Figure 6: Evolution of u_x, v_x and w_x errors with the both methods.

7 degrees for the non linear optimization process.

Globally, the simultaneous estimation of X and T is more accurate than the non linear optimization technique and seems to resist in a better way to the various type of noise affecting the whole hand-eye calibration process.

4 Real Experiments

A real hand-eye calibration had been performed using the Cartesian robot of the laboratory. This robot has 6 degrees of freedom and moves in a work volume of about $1.5m \times 1.5m \times 1.0m$.

The principle of the calibration set-up is similar to the procedure described in the previous section. However, the set of gripper motions do not correspond to fixed trajectories but, is chosen so that the robot movements magnitudes are as large as possible for each degree of freedom.

The calibration object sits in the middle of the robot workspace and is visible at each gripper station.

For this experiment, the robot camera had been fitted out with a *fish-eye* lens. This kind of lens presents a very significant radial distortion. Intrinsic calibration of the vision system was performed and radial distortion defects corrected for the whole set of images. We have assumed that all other optical deformations were negligible.

Since we can't know a priori the numerical values of X and T parameters, the estimation accuracy has been checked out by moving the robot camera. Using this method enables to test independently each estimated parameter of X.

This verification includes two parts and requires a particular set-up described as follows (see fig.7).

The robot camera is placed at about $50cm$ of a perforated wood plate (with a hole of $1cm$ diameter). A LED is fixed on the robot superstructure at about $1.2m$ behind the plate. The robot camera, the LED and the wood plate are then situated in a configura-

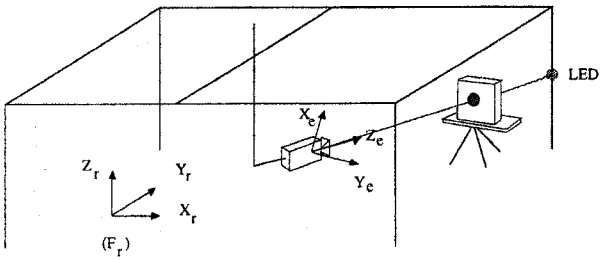

Figure 7: Schema of the verification experiment set-up.

tion where the LED is visible through the hole. This causes the LED, the hole and the camera optical center O_e to be aligned.

Knowing the X transformation allows to move directly the camera instead of the gripper inside the robot workspace. If intrinsic calibration is rightly performed and therefore X is precisely identified, changing the camera orientation by rotating around one of the F_e axes will not perturb the alignment and the LED will remain visible through the plate hole.

Figure 8 illustrates this part of the verification experiment. It is composed of 5 images representing a detail of the scene after each camera motion. These details are centered on the LED spot. The complete viewpoints at each position of the verification experiment can be seen in fig.12. The rotation angles magnitudes have been limited so that the plate remains in the camera's view. However, the very small focal length of the *fish-eye* (about 500 pixels) has to be noticed and it causes the intervals of robot rotation angles to be relatively large: about 60^o for the rotation around X_e, 80^o for the rotation around Y_e and 120^o for the rotation around Z_e. In each image, the LED is visible through the plate hole. The alignment is respected and therefore the rotational part of X has acceptable values.

In the second part of the verification experiment, the robot camera was placed so that the LED image was located at the image center, denoted (u_0, v_0).

It is the intersection between the optical axis Z_e and the image plane. (u_0, v_0) has been performed by intrinsic calibration. Let (u_e, v_e) be the image coordinate frame. u_e and v_e are parallel to X_e and Y_e respectively. Under these conditions, translating the robot camera along the X_e or the Y_e axis will cause the spot representing the LED image to move in the image plane on a straight line parallel to u_e or v_e and passing through (u_0, v_0).

Note that the lens distortion is supposed to be only radial and doesn't have any effect on the spot location since it belongs to a straight line passing through the image center.

Translating the robot camera along the Z_e axis will cause the LED spot to remain located at (u_0, v_0).

Figures 9 to 11 show the different steps of this second verification part. As for fig.8, they represent only details. The global views can be seen in fig.13 to 15. Two lines passing through (u_0, v_0) and parallel to the image frame axes have been superimposed to the series of test images. The spot moves along this lines when the camera is translated along the X_e and Y_e axes. The only deviations worthy to notice are about a few pixels. Similarly, when the camera is translated along the Z_e axis, the spot remains roughly centered in the image plane. It proves that the estimation of the translation components of X is also quite accurate.

5 Conclusion

This paper has addressed the issue of the hand-eye calibration problem. We have explained and developed a new formulation which is based on the non linear minimization of a sum of scalar products.

The major peculiarity of this new method is the simultaneous estimation of the hand-eye transformation X and the calibration object location T. In opposition to the previous existing techniques, the number of parameters to be estimated do not depend on the number of gripper stations and image acquisitions, but remains equal to 12. Moreover, the simultaneous estimation of transformation T introduces a significant constraint and ensures X and T to be consistent with the set of calibration data.

Tests with simulations and real experiments showed the reliability of the process. Comparisons with the non linear optimization technique have been performed and prove that the simultaneous estimation of X and T resists in a better way to the increase of noise in simulation data and yields to more accurate results.

Special conditions aren't required for the gripper movements and for the location of the calibration object with respect to the camera. But, intrinsic calibration must be performed before using this method. The process can be easily implemented and the calibration is quite fast.

However, the simultaneous estimation of X and T will be further improved in real experiments. Tests have been already performed with two types of optical systems, several sets of gripper and calibration object positions and different kinds of calibration objects. They all led to very accurate results. We attempt now to improve the reliability of this new algorithm by enhancing the extraction of the feature points and optimizing the set of gripper positions in order to constraint the hand-eye calibration parameters in a better way.

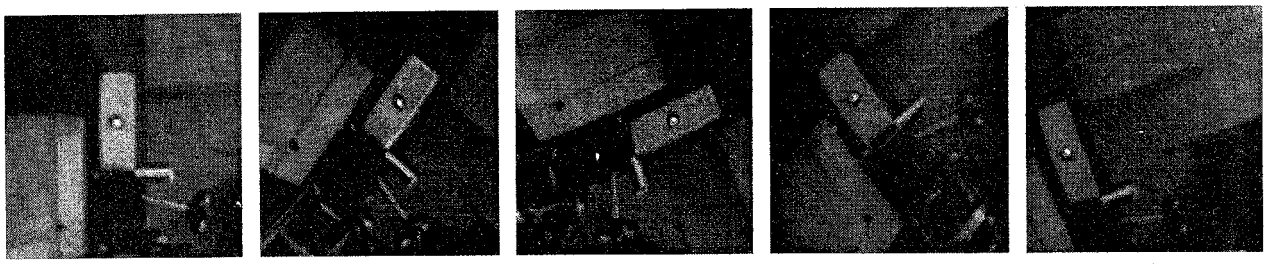

start view (1) (2) (3) (4)

Figure 8: Views of the spot through the plate hole while rotating around F_e axes.

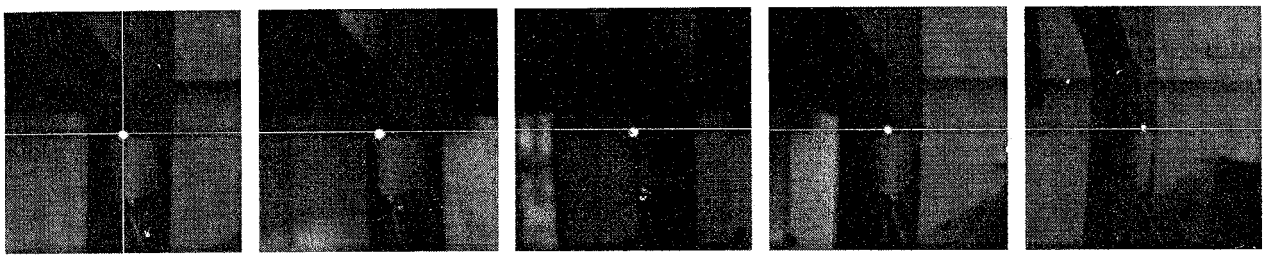

start view $X_e = 0$ $X_e \simeq 40cm$ $X_e \simeq 80cm$ $X_e \simeq -40cm$ $X_e \simeq -80cm$

Figure 9: Views of the spot while translating along X_e axis: the total distance covered by the camera is about $1.6m$.

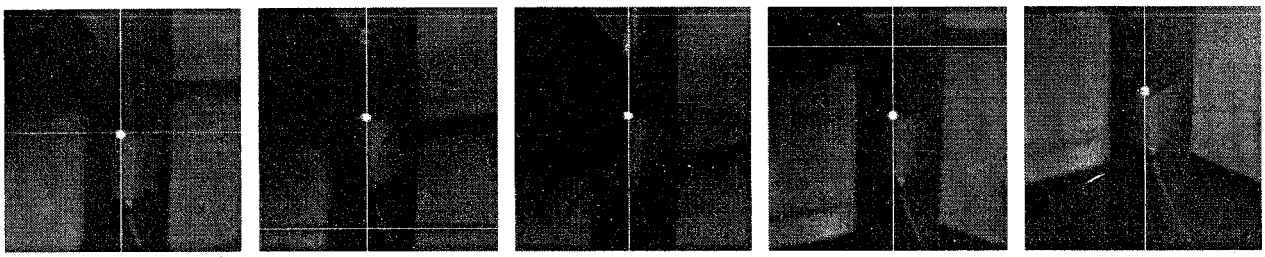

start view $Y_e = 0$ $Y_e \simeq 15cm$ $Y_e \simeq 30cm$ $Y_e \simeq -15cm$ $Y_e \simeq -30cm$

Figure 10: Views of the spot while translating along Y_e axis: the total distance covered by the camera is about $60cm$.

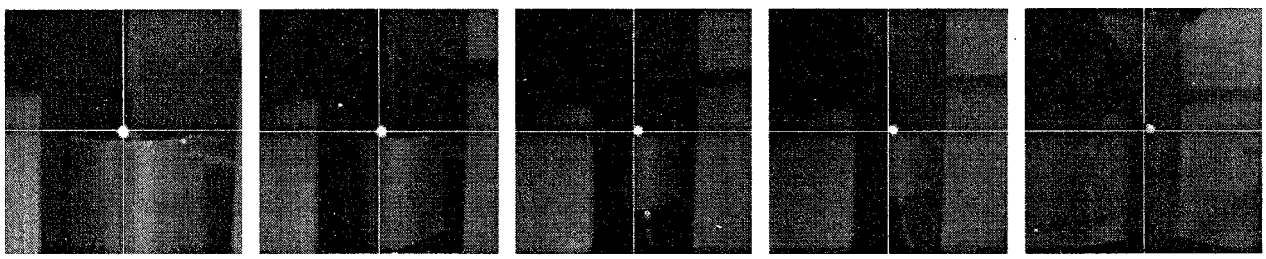

start view $Z_e = 0$ $Z_e \simeq 30cm$ $Z_e \simeq 60cm$ $Z_e \simeq 90cm$ $Z_e \simeq 1.2m$

Figure 11: Views of the spot while translating along Z_e axis: the total distance covered by the camera is about $1.2m$.

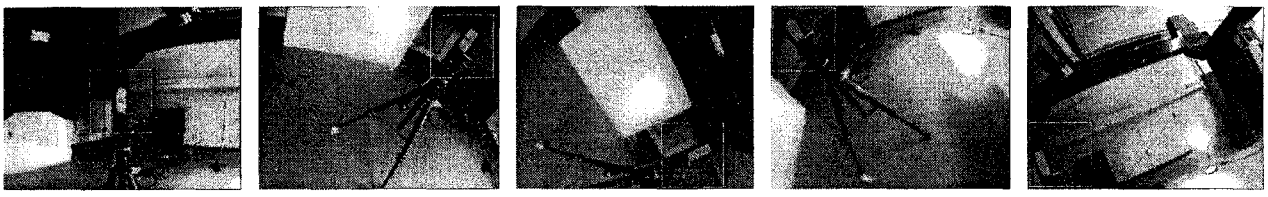

start view (1) (2) (3) (4)

Figure 12: Complete viewpoints while rotating around F_e axes.

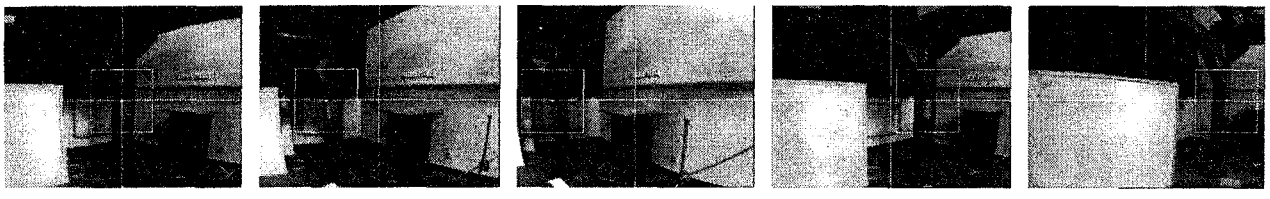

start view (1) (2) (3) (4)

Figure 13: Complete viewpoints while translating along X_e axis.

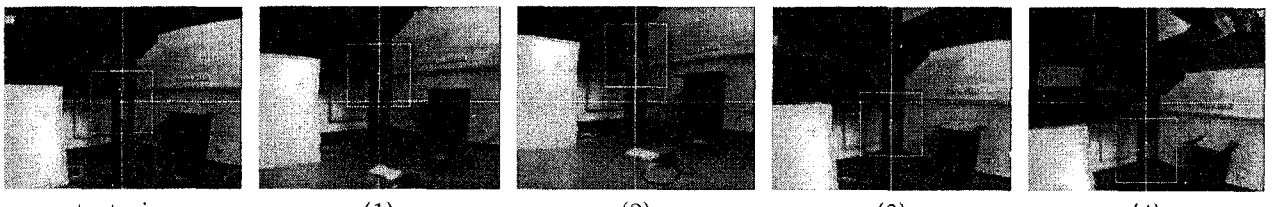

start view (1) (2) (3) (4)

Figure 14: Complete viewpoints while translating along Y_e axis.

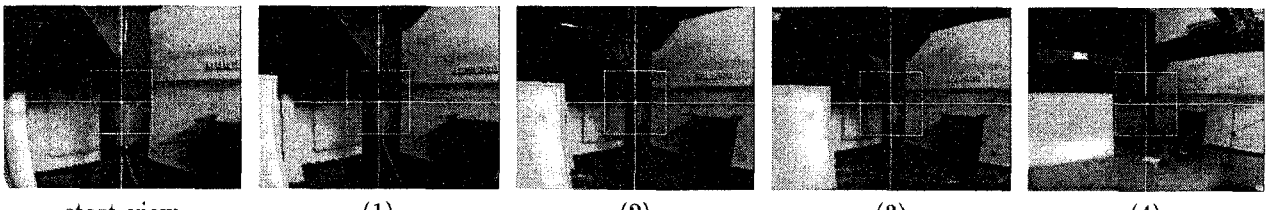

start view (1) (2) (3) (4)

Figure 15: Complete viewpoints while translating along Z_e axis.

References

[1] R. Horaud and F. Dornaika. Hand-Eye Calibration. In *Workshop on Computer Vision for Space Applications*, pages pp.369–379, Antibes, France, sept. 1993.

[2] Y.C. Shiu and S. Ahmad. Calibration of Wrist-Mounted Robotic Sensors by Solving Homogeneous Transform Equations of the Form AX = XB. *IEEE Transactions on Robotics and Automation*, 5(1):pp.16–29, February 1989.

[3] R.Y. Tsai and R.K. Lenz. A New Technique for Fully Autonomous and Efficient 3D Robotics Hand/Eye Calibration. *IEEE Transactions on Robotics and Automation*, 5(3):pp.345–358, June 1989.

[4] C-C. Wang. Extrinsic Calibration of a Vision Sensor Mounted on a Robot. *IEEE Transactions on Robotics and Automation*, 8(2):pp.161–175, April 1992.